Journal of Hazardous Materials 250–251 (2013) 318–332

Contents lists available at SciVerse ScienceDirect

Journal of Hazardous Materials

journal homepage: www.elsevier.com/locate/jhazmat

Phytotoxic hazards of NiO-nanoparticles in tomato: A study on mechanism of cell death

Mohammad Faisal[a,1], Quaiser Saquib[b,1], Abdulrahman A. Alatar[a], Abdulaziz A. Al-Khedhairy[b], Ahmad K. Hegazy[a,c], Javed Musarrat[d,*]

[a] Department of Botany & Microbiology, College of Science, King Saud University, P.O Box 2455, Riyadh 11451, Saudi Arabia
[b] Department of Zoology, College of Science, King Saud University, P.O. Box 2455, Riyadh 11451, Saudi Arabia
[c] Department of Botany, Faculty of Science, Cairo University, Giza, Egypt
[d] Department of Agricultural Microbiology, Faculty of Agricultural Sciences, AMU, Aligarh 202002, India

HIGHLIGHTS

- First report on mechanism of NiO-NPs induced apoptosis in tomato roots cells.
- NiO-NPs trigger the release of caspase-3 proteases from mitochondria.
- Flow cytometry data validated oxidative burst and mitochondrial dysfunction.
- NiO-NPs at varying concentrations induced imbalance in antioxidant enzymes.
- Damage to DNA signifies the toxic potential of NiO-NPs to plants.

ARTICLE INFO

Article history:
Received 23 October 2012
Received in revised form 20 January 2013
Accepted 25 January 2013
Available online xxx

Keywords:
Nickel oxide nanoparticles
DNA damage
Apoptosis
Oxidative stress
Phytotoxicity

ABSTRACT

Nickel oxide nanoparticles (NiO-NPs) in the concentration range of 0.025–2.0 mg/ml were examined for the induction of oxidative stress, mitochondrial dysfunction, apoptosis/necrosis in tomato seedling roots, as an in vivo model for nanotoxicity assessment in plants. Compared to the control, catalase (CAT), glutathione (GSH), superoxide dismutase (SOD) and lipid peroxidation (LPO) in 2.0 mg/ml NiO-NPs treatments exhibited 6.8, 3.7, 1.7 and 2.6-fold higher activities of antioxidative enzymes. At 2.0 mg/ml, 122% and 125.4% increase in intracellular reactive oxygen species (ROS) and mitochondrial membrane potential ($\Delta\Psi m$) of seedling roots confirmed the oxidative stress and mitochondrial dysfunction. Comet assay exhibited a significant increase in the number of apoptotic (21.8%) and necrotic (24.0%) cells in 2.0 mg/ml treatment groups *vis-á-vis* in control 7% apoptotic and 9.6% of necrotic cells were observed. Flow cytometric analysis revealed 65.7% of apoptotic/necrotic cell populations and 2.14-fold higher caspase-3 like protease activity were recorded in 2.0 mg/ml treatment groups. Ultrastructure analysis revealed NiO-NPs translocation, nuclear condensation, abundance in peroxisomes and degenerated mitochondrial cristae. The dissolution of Ni ions from NiO-NPs signifies its potential to induce cell death presumably by Ni ions, triggering the mitochondrial dependent intrinsic apoptotic pathway.

1. Introduction

The widespread application of nanotechnology based consumer products has raised concern over the impact of nanoparticles (NPs) on the environment and on biota; therefore, release of NPs into the environment is likely inevitable [1]. Plant communities play a critical role in the sustenance of ecosystem, and as such, may experience significant exposure to NPs [2,3]. NPs can enter into plant cells either through endocytosis or non-endocytic penetration [4,5]. NPs can be taken up by plant roots and transported to shoots through vascular systems depending upon the composition, shape, size of NPs and plant anatomy. Cellular uptake of zinc oxide (ZnO) is reported in *Lolium perenne* [5], Cu-NPs in *Phaseolus radiates* and *Triticum aestivum* [6], multiwalled carbon nanotubes (MWCNTs) in *Oryza Sativa* [4], *Triticum aestivum* [7] and CdSe/ZnS quantum dots in *Poa annua* [8]. Lin and Xing [9] has studied the effect of MWCNT, Al, Al_2O_3, Zn and ZnO-NPs on seed germination and root elongation in *Brassica napus*, *Raphanus sativus*, *Lolium perenne*, *Lactuca sativa*, *Zea mays* and *Cucumis sativus*. At 2000 mg/L,

* Corresponding author at: Department of Zoology, College of Science, P.O. Box 2455, King Saud University, Riyadh 11451, Saudi Arabia. Tel.: +966 4675768; fax: +966 4675514.
E-mail address: musarratj1@yahoo.com (J. Musarrat).
[1] These authors contributed equally to this work and considered as first authors.

0304-3894/$ – see front matter © 2013 Elsevier B.V. All rights reserved.
http://dx.doi.org/10.1016/j.jhazmat.2013.01.063

non-significant effect was observed on seed germination except for the Zn-NPs on *Lolium perenne* and ZnO-NPs on *Zea mays*. However, inhibition on root growth varied greatly among NPs and plants. At the similar concentration the Zn-NPs and ZnO-NPs practically terminated root elongation of the tested plant species. Cañas et al. [10] have studied the effects of non-functionalized single-walled carbon nanotubes (SWCNTs) and functionalized (fSWCNTs) on root elongation of *Brassica oleracea*, *Daucus carota*, *Cucumis sativus*, *Lactuca sativa*, *Allium cepa* and *Lycopersicon esculentum*. Both SWCNTs and fSWCNTs affected root elongation of four crop species, but phytotoxicity varied between SWCNTs and fSWCNTs, with SWCNTs affecting more species. These effects of nanomaterials are most often associated with the increased reactivity and surface area, ROS formation, aggregation and adsorption to cell walls, and release of toxic ions [3,11]. In a recent report, exposure of *Arabidopsis thaliana* roots to 100 mg/L ZnO, TiO_2-NPs and fullerene soot exhibited up and down-regulation of an array of genes related to stress response, including both abiotic (oxidative, salt, water deprivation) and biotic (wounding and defense to pathogens) [1]. The accumulation, persistence and impact of NPs on plant metabolism and development depend on the hydrodynamic size, concentration, surface chemistry of NPs, and the chemical milieu of the sub-cellular sites of NPs deposition [12]. Most likely, the NPs interact with biological systems through the (i) chemical effects as metal ions in solution upon dissolution; (ii) mechanical effects owing to hard spheres and defined interfaces; (iii) catalytic effects on surfaces; (iv) binding with macromolecules either by non-covalent or covalent mechanisms; and (v) intracellular oxidative stress [12]. Toxic metals, such as Cu, Cd, Hg, Ni and Zn, bind to cell components such as DNA or the sulfhydryl, carboxyl or imidazole groups of proteins, and modify their activities. Interference with cellular processes often causes redox imbalances and oxidative stress in metal-exposed plants [13,14]. The ability of NPs to enter the nuclear envelope has also evoked much interest in possible genotoxic effects of NPs [15]. Apart from direct intercalation or the physical and/or electrochemical interaction with NPs, ROS are regarded as key factor in inducing DNA damage [16]. There is ample evidence that ROS are crucial second messengers involved in abiotic and biotic stress in plants [17,18], and also participate as important signaling molecules for controlling plant programmed cell death (PCD) [19]. ROS include the superoxide radical ($O_2^{\bullet -}$), hydroxyl radical ($OH^{\bullet}$), hydroperoxyl radical ($HO_2^{\bullet}$), hydrogen peroxide (H_2O_2), alkoxy radical ($RO^{\bullet}$), peroxy radical ($ROO^{\bullet}$), singlet oxygen ($^1O_2$) and excited carbonyl (RO^*), all of which are cytotoxic to plants [20]. ROS can attack virtually all macromolecules, which results in serious damage to cellular components, DNA lesions and mutations, and this often leads to irreparable metabolic dysfunction and cell death [20]. Reduced levels of ROS stimulate Ca^{2+} influx into the cytoplasm and activate NADPH oxidase. Plant NADPH oxidases generate $O^{2\bullet -}$, which gets converted to H_2O_2 by SOD and the peroxide diffuses through the cell wall to the extracellular medium and enters into the cell [21]. H_2O_2 is one of the most stable ROS reported to trigger apoptotic cell death in cultured tobacco BY-12 cells [22,23]. Numerous apoptosis-inducing agents can induce the uncoupling of electron transport for ATP production, leading to a decrease in $\Delta\Psi m$ and subsequent ROS formation. ROS are also considered as the main underlying chemical process in nanotoxicology, leading to secondary processes that can cause cellular damage and eventually cell death [24]. Many features of PCD in plants resemble with those observed in animals with respect to similarities in plant DNA sequences, apoptosis-related genes, processing of the DNA and rupture of the nuclei, shared by both types of cell death processes [25]. However, the mechanism of DNA damage, ROS generation and activation of cell signaling pathways for NPs induced oxidative stress leading to phytotoxicity is not fully understood. Therefore, the objective of this study was to investigate the nickel oxide (NiO-NPs) induced phytotoxicity in tomato (*Lycopersicon esculentum*) seedlings roots, and assess the (i) translocation of NiO-NPs in root cells and ultrastructural changes in cell organelles, (ii) potential of NiO-NPs to release Ni ions and their role in intracellular ROS generation to induce mitochondrial dysfunction, (iii) levels of oxidative stress marker enzymes, (iv) cell cycle alterations and apoptosis/necrosis analysis by use of highly sensitive techniques. To the best of our understanding, no systematic study has been attempted so far, elucidating the mechanism of NiO-NPs induced phytotoxicity at cellular and molecular levels. This study will help in understanding the impact of NiO-NPs on the growth of tomato seedling roots, level of oxidative stress, dissipation of $\Delta\Psi m$, and release of caspase-3 like protease, leading to ROS mediated induction of mitochondrial dependent intrinsic apoptotic pathway.

2. Experimental

2.1. Characterization of NiO-NPs

NiO-NPs were characterized by TEM, atomic force microscopy (AFM), dynamic light scattering (DLS) and zeta (ζ) potential measurements. For TEM analysis, the samples were prepared by dropping the ultrasonically treated NiO-NPs suspension onto a TEM copper grid and dried at room temperature. A total of six TEM samples were prepared, and at least ten micrographs of each were analyzed to determine the average primary particle size. TEM was performed on a Field Emission Transmission Electron Microscope (JEM-2100F, JEOL, Japan) at 200 keV. NiO-NPs were further examined using AFM (Veeco Instruments, USA). Analysis was performed by running the machine in non-contact tapping mode. Characterization of NiO-NPs was done by observing the patterns appeared on the surface topography and analyzing the AFM data. Tapping mode imaging was implemented in ambient air by oscillating the cantilever assembly at or near the cantilever's resonant frequency using a piezoelectric crystal. The topographical images were obtained in tapping mode at a resonance frequency of 218 kHz. NiO-NPs stock suspension of 20 μg/ml was prepared in deionized ultrapure water and sonicated for 15 min at 40 W. DLS was performed on a ZetaSizer-HT, Malvern, UK to determine the hydrodynamic sizes of the NiO-NPs in suspension. The ζ-potential values of the NiO-NPs were determined by Zetasizer 2000 (Malvern instruments Ltd., UK). The NiO-NPs were dispersed in ultrapure water and the ζ-potential values presented were the average of 10 readings.

2.2. Effect of NiO-NPs and bulk NiO on root elongation

Tomato seeds (super strain B) were sterilized using 5% clorox solution for 10 min and thoroughly washed with ultrapure water. The exposure concentrations of NiO-NPs were selected from initial experiments based on the root elongation assay. In brief, for each set of experiment, 20 sterile seeds were separately dipped in 0.025, 0.05, 0.1, 0.25, 0.5, 1.0, 1.5 and 2.0 mg/ml of NiO-NPs ($\leq$50 nm) (catalog no. 637130, Sigma Chemical Company, St. Louis, MO, USA) and bulk NiO (catalog no. 203882, Sigma Chemical Company, St. Louis, MO, USA) suspensions, exposure was done for 2 and 4 h on a rotary shaker at room temperature. After the treatment, seeds were rinsed with ultrapure water and transferred onto wet filter paper in Petri dishes and placed in growth chamber for 5 and 10 days at 25 ± 2 °C for seed germination and growth.

2.3. Translocation of NiO-NPs in tomato root cells

TEM analysis of tomato seedling roots from NiO-NPs (2.0 mg/ml) treatment groups were analyzed for uptake and translocation of NPs following the method described by Corredor et al. [26]. Briefly,

roots from untreated control and NiO-NPs treatment groups were fixed with 10% glutaraldehyde in 0.1 M cacodylate buffer (pH 7.4) for 20 min. Roots were then suspended in 1% OsO4 in 0.1 M cacodylate buffer (pH 7.4) for 1 h at 4 °C, followed by 1 h incubation in 2% aqueous uranyl acetate at room temperature. The samples were dehydrated in an ethanol series and embedded in low viscosity araldite resin. Ultrafine sections (80 nm thick) were visualized under high vacuum at 100 kV using JEOI-1011 Electron Microscope (JEOL, Tokyo, Japan). The images were captured without any contrast agent to avoid potential artifacts due the deposition of contrast agent crystals.

2.4. Dissolution of NiO-NPs and bulk NiO in treatment solutions

Concentrations of total dissolved Ni ions in NiO-NPs and bulk NiO treatment solutions were measured to assess the role of soluble metal in phytotoxicity. Assessment of dissolved Ni ions was measured following the method described by Lee et al. [27]. In brief, NiO-NPs and bulk NiO suspensions (250, 1000 and 2000 mg/L) were centrifuged at 12,000 × *g* for 20 min. The supernatants were subsequently filtered through 0.22 μm syringe filters and subjected to elemental analyses of Ni ions by inductively coupled plasma optical emission spectrometry (ICP-OES, PerkinElmer Optima 4300DV, USA).

2.5. NiO-NPs induced ROS generation

Qualitative analysis of ROS production were done by staining the seedling roots with 0.25 μM of 2′,7′-dichlorofluorescin diacetate (DCFH-DA) for 15 min and images were taken using a fluorescence microscope (Nikon Eclipse 80i, Japan) [28]. For the quantitative estimation of intracellular ROS, protoplasts were isolated by the method of Imanishi et al. [29] and staining with 5 μM of DCFH-DA. Fluorescence of DCF from 50,000 protoplasts was recorded on Beckman Coulter flow cytometer (Coulter Epics XL/Xl-MCL, USA) following our method, as described previously [30].

2.6. Effect of NiO-NPs on $\Delta\Psi m$

Visual changes in $\Delta\Psi m$ was done by staining the seedling roots with 1 μg/ml of Rh123 for 30 min in dark and the images were taken on a fluorescence microscope. Quantitation of intracellular alterations in $\Delta\Psi m$ was done on flow cytometer by analyzing 50,000 protoplasts from different treatment groups stained with Rh123 (5 μg/ml) following our method, as described previously [31].

2.7. Biochemical assays

CAT (catalog # 707002), GSH (catalog # 703002), SOD (catalog # 706002) and LPO (catalog # 705002) in control and NiO-NPs treatment groups were measured in tissue extracts of 20 seedling roots following the manufacturers protocol (Cayman Chemicals, MI, USA). The resulting colored compounds were measured on multiwell microplate reader (Multiskan Ex, Thermo Scientific, Finland) at 550, 405, 450 and 500 nm, respectively.

2.8. Isolation of nuclei

In brief, 20 roots obtained from seedlings of control and NiO-NPs treated groups were placed in 60-mm Petri dish on ice containing 1 ml of Galbraith buffer (45 mM $MgCl_2$, 30 mM sodium citrate, 20 mM MOPS, 0.1% (v/v) Triton X-100, pH 7.0). Roots were gently sliced in the buffer using new razor blades keeping the dish slightly tilted so that nuclei can pass into the buffer. To remove the debris, nuclei suspension was filtered through a 28-μm nylon filter mesh.

2.9. Apoptosis and necrosis analysis by alkaline comet assay

Alkaline comet assay were performed with the isolated nuclei, following our previously described method [32]. A separate solution of EMS (2 mM) was prepared as a positive control. Acellular treatment of nuclei with EMS was done by immersing the two extra slides prepared from control groups in EMS solution for 2 h at room temperature. The cells for apoptotic and/or necrotic DNA were analyzed following the scoring criteria of Singh [33]. Percentage of nuclei with radially diffused (necrotic) and hazy outline (apoptotic) DNA was separately calculated from a total of 1000 nuclei (500 nuclei from each replicate slide).

2.10. Analysis of apoptosis by flow cytometry

The assessment of apoptosis was performed by use of flow cytometry following our previously described methods [31,34]. In brief, the aliquots of 1 ml nuclei suspensions were stained in dark with 50 μg/ml of nuclear staining fluorescent dye (propiodium iodide, PI) and RNAase A (50 μg/ml) solutions for 10 min on ice to degrade the RNA in test samples. Fluorescence intensities of 100,000 nuclei were acquired by use of a Beckman Coulter flow cytometer.

2.11. Measurement of caspase-3 like protease activity

Cleavage product of caspase-3 was detected in seedling roots (200 mg) from control and NiO-NPs treatment groups by ELISA using the caspase-3/CPP32 colorimetric assay kit (catalog # K106-25, Biovision, CA, USA). The colored formation of p-nitroanilide was measured at 405 nm by use of a microplate reader.

2.12. Statistical analysis

Data were expressed as mean ± S.D. for the values obtained from at least three independent experiments using 20 seeds/concentration. Statistical analysis was performed by one-way analysis of variance (ANOVA) followed by Dunnett's multiple comparisons test.

3. Results and discussion

3.1. Particle characterization by TEM, AFM, DLS and zeta (ζ)-potential measurements

In order to investigate the morphology and size, NiO-NPs in the solid state were investigated by TEM, AFM and also in aqueous suspension by DLS measurements. The TEM analysis of NiO-NPs showed that most of the particles were crystallites spheres with polyhedral morphologies and forming agglomerates. The size of the particles was wide with the average size of 23.34 nm (Fig. 1A). AFM image of NiO-NPs exhibited the size of nanoparticles to be 30 nm (Fig. 1B). The distribution curves in water show particle aggregates of 239.8 ± 4.1 nm. The result of hydrodynamic size of the NiO-NPs using DLS is shown in Fig. 1C. The ζ-potential for NiO-NPs in water was found to be 25.3 ± 1.2 mV (Fig. 1D). The commercially available NiO-NPs (<50 nm), suspended in water were used for seed treatment and subsequent analysis of toxicity in tomato root cells. Since, the primary and secondary sizes of the NPs are regarded as important parameters for cellular toxicity. Therefore, the behavior of NiO-NPs in treatment solution was evaluated through DLS to understand the extent of aggregation and secondary size of these NPs before exposure. DLS is widely used to determine the size of Brownian NPs in colloidal suspensions in the nano and submicron ranges [35]. The average hydrodynamic particles diameter in water indicates particle aggregation. The hydrodynamic characterization

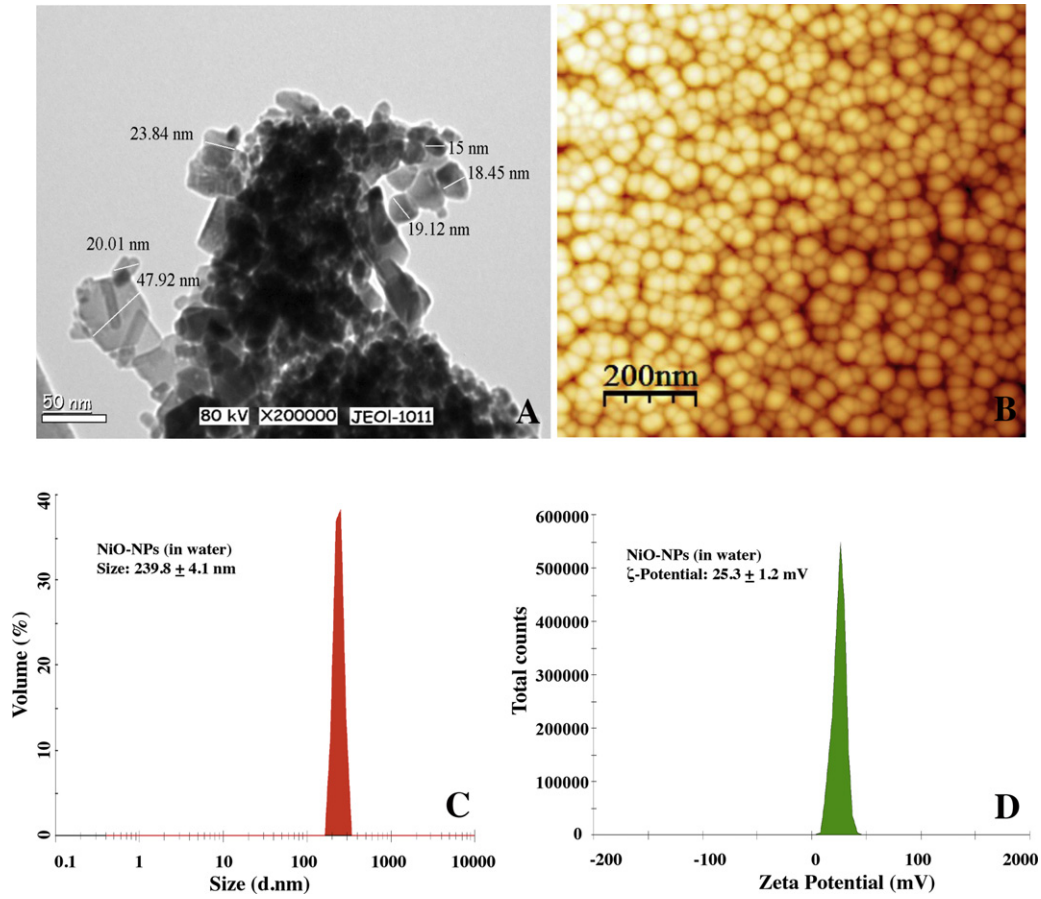

Fig. 1. Representative TEM image of NiO-NPs (panel A) at 200,000× magnification. Panel B depicts a 3D topography of NiO-NPs in an AFM perspective view with scan size of 200 nm. Dynamic light scattering (DLS) and ζ-potential analysis of NiO-NPs suspension in ultrapure water (panels C and D).

data corroborates well with some recent reports on the agglomeration of TiO_2, ZnO and superparamagnetic iron oxide-NPs in aqueous environment [30,36,37].

3.2. Repression of root length by NiO-NPs exposure

A comparative study on root elongation has been done to assess the phytotoxicity of NiO-NPs and bulk NiO in tomato. Exposure concentrations for NiO-NPs were selected based on the screening of low to high concentrations (0.025–2.0 mg/ml) of NiO-NPs to affect the root length. We observed significant enhancement in root length treated with 0.05 and 0.1 mg/ml. Since, the primary objective of this study was to assess the toxicity of NiO-NPs. Therefore, the non-significant concentrations (0.025–0.1 mg/ml) in term of repression of root length were excluded from further toxicity experiments. Tomato seeds exposed to NiO-NPs for 2 and 4 h, exhibited a concentration dependent reduction in root length (Fig. 2). After 5 days of incubation, at the highest concentration of 2.0 mg/ml, the average root length in 2 and 4 h treatment groups were repressed to 0.8 ± 0.22 and 0.5 ± 0.12 cm ($p < 0.01$) *viz-á-viz* the root length in untreated controls were determined to be 3.8 and 3.9 cm, respectively. Under similar experimental conditions bulk NiO did not induce significant change in the root length (Fig. S1 Supplementary data). Within 2 h treatment groups, seedlings left for 10 days exhibited normal root growth upto the concentrations of 1.0 mg/ml. Stunted roots were observed only at 1.5 mg/ml and termination of root elongation was observed at 2.0 mg/ml. On the contrary, 10 days old seedlings in 4 h treatment groups exhibited greater toxicity as observed by the complete death of roots at 1.0, 1.5 and 2.0 mg/ml (data not shown). Our results corroborate the earlier studies, which have also suggested the retardation of root growth by Zn, ZnO, SWCNTs, Cu and TiO_2-NPs in *Lycopersicon esculentum*, *Raphanus sativus*, *Brassica napus*, *Lolium perenne*, *Cucurbita pepo* and *Oryza sativa* [5,10,38,39]. Water soluble fullerene has also been reported to retard roots length and loss of root gravitropism in *Arabidopsis thaliana* [40]. Conversely, there are also reports, which have suggested that the NPs such as MWCNT and TiO_2, can penetrate into *Nicotiana tabacum*, *Lycopersicon esculentum* and aged *Spinacia oleracea* seed coats, and dramatically enhance their

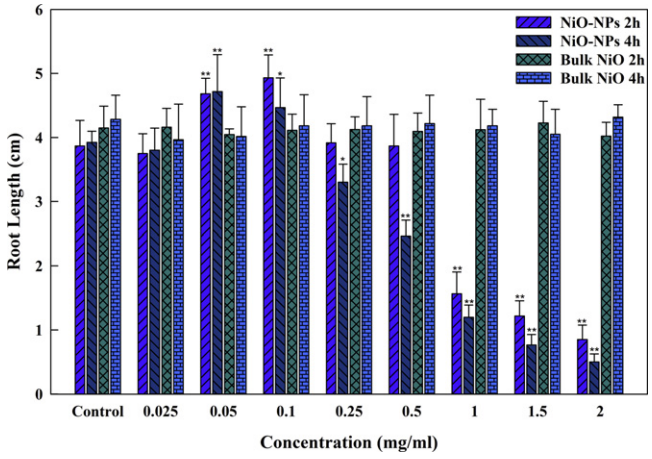

Fig. 2. Concentration dependent effect of NiO-NPs and bulk NiO on repression of tomato roots after 5 days ($^{*}p < 0.05$, $^{**}p < 0.01$ vs. control).

germination and root elongation at concentration ranges of 5–500 and 10–40 μg/ml, respectively [41–43].

Toxicity assessment of NPs on plant system is still emerging and the available data are primarily based on conventional tests suggested by the United States Environment Protection Agency [44] including seed germination, root elongation, biomass changes and histological studies. These tests provide only the symptomatic information related to the possible toxicity of nanomaterials. To the best of our knowledge, this study for the first time investigated the mechanistic aspects of NiO-NPs induced oxidative stress and apoptosis in tomato. For this purpose, tomato was taken as a model because of its economic importance and sensitivity toward NPs exposure [41]. Although, the selective permeability of seed coat provides protection to the seed from NPs during the germination, but our results demonstrated that the embryonic root (radicle) after penetrating the seed coat, become the major organ to confront NiO-NPs during the seedling growth. Therefore, the toxic symptoms were more evident in roots than in other parts of seedlings.

Furthermore, NiO-NPs also exhibited a tendency to adsorb on the seed coat in a concentration dependent manner (Fig. S2 Supplementary data). The main factors contributing to such adsorption can be physical attachment of particles on a rough seed surface, electrostatic attraction and hydrophobic interactions between seeds and NP agglomerates. The adsorption of NPs on the seed surface could generate locally concentrated ions (released from NPs) and enhance NP phytotoxicity [45]. Thus, it is concluded that the

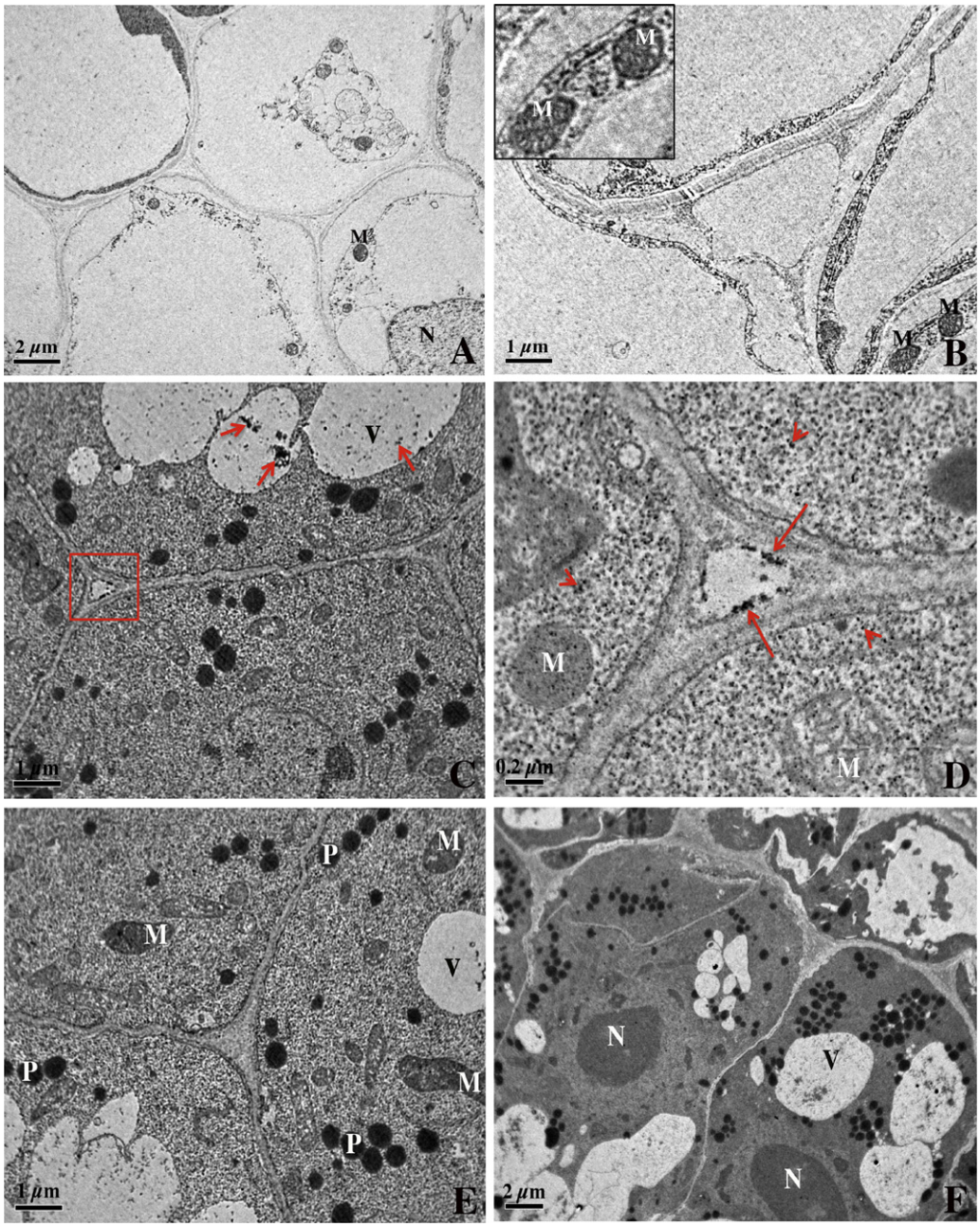

Fig. 3. TEM images of control roots showing the parenchymal cells harboring mitochondria with integrated cristae, nuclear chromatins at the peripheral region and no peroxisomes (panels A and B). Ultrastructure image of roots from 2.0 mg/ml NiO-NPs treatment group showing the presence of NiO-NPs aggregates (marked within box) in triangle shaped extracellular region between three confluent parenchymatic cells (panel C) and vacuoles (arrows). High magnification of the extracellular channel displaying NPs aggregates (marked with arrows) in panel C and presence of NPs inside the cytoplasm (arrow heads) (panel D). Panel E depicts mitochondria with degenerated cristae and abundance of peroxisomes. Panel F depicting the nuclear condensation. Vacuoles (V), mitochondria (M), peroxisomes (P), and nucleus (N).

effect of NPs on plant growth and development depends upon the type and concentration of NPs, plant species and their mode of NPs uptake.

3.3. Ultrastructure analysis and dissolution of Ni ions

Ultrastructure analysis was performed to evaluate the translocation of NiO-NPs in root tissues. TEM analysis showed that NiO-NPs not only present in the exterior region of confluent parenchymal cells but also translocated within the cytoplasm of the cells (Fig. 3A and B). NPs presence was identified as dark dots and aggregates in the vacuoles of root cells. It suggests that NPs successfully pierced the seed coat and cross the cell membrane and formed agglomerates. Translocation of NiO-NPs in root cells is supported by ZnO and carbon coated iron-NPs uptake in *Fagopyrum esculentum* and *Cucurbita pepo* [26,46]. Additionally, we also observed an increase in the number of peroxisomes and mitochondria with degenerated cristae, and nuclear condensation in root cells of NiO-NPs treatment group (Fig. 3C and D). Through electron microscopic analysis, ozone, herbicide, clofibrate, and high light were found to increase peroxisome abundance in plant cells [47–50]. In addition to the metabolic pathways and division factors that link peroxisomes and mitochondria, other ways of interaction or communication also exist between these two organelles. For instance, in yeast, mitochondrial dysfunction induces peroxisome biogenesis and increases peroxisomal functions via a retrograde signaling pathway controlled by the transcription factor RTG [51,52]. Our study supports the view that NiO-NPs induced mitochondrial dysfunction has triggered the biogenesis of peroxisomes as a consequence of stunted root growth and to detoxify the intracellular ROS.

Table 1
Total dissolved Ni ions released from NiO-NPs and bulk NiO particles suspended in ultrapure water.

NiO added (mg/L)	Total dissolved Ni (mg/L)	
	NiO-NPs	Bulk NiO
0	N.D.	N.D.
250	2.31 ± 0.45^{b}	$0.6 \pm 0.03^{c,d}$
1000	2.97 ± 0.57^{b}	0.38 ± 0.05^{d}
2000	11.37 ± 0.98^{a}	1.47 ± 0.19^{c}

Values represent mean ± S.D. Means followed by the same letter are not significantly different ($P < 0.05$) using Tukey's test. N.D., not detected.

Quantitative estimation of dissolved Ni ions in both NiO-NPs and bulk NiO treatment solutions was done by ICP analysis. Compared to the bulk NiO, a remarkable increase in the level of dissolved Ni ions were recorded in NiO-NPs solutions. Bulk NiO and NiO-NPs at the highest concentration of 2000 mg/L released 1.472 ± 0.192 and 11.37 ± 0.98 mg/L of Ni ions (Table 1). For Ni ions the possible mode of action to cause DNA damage has been reported by inducing the Haber–Weiss generation of •OH radical [53,54]. Therefore, the possibility cannot be ruled out that NiO-NPs translocated within the root cells releases Ni ions and assist the intracellular ROS production which induce damage to the biological macromolecules.

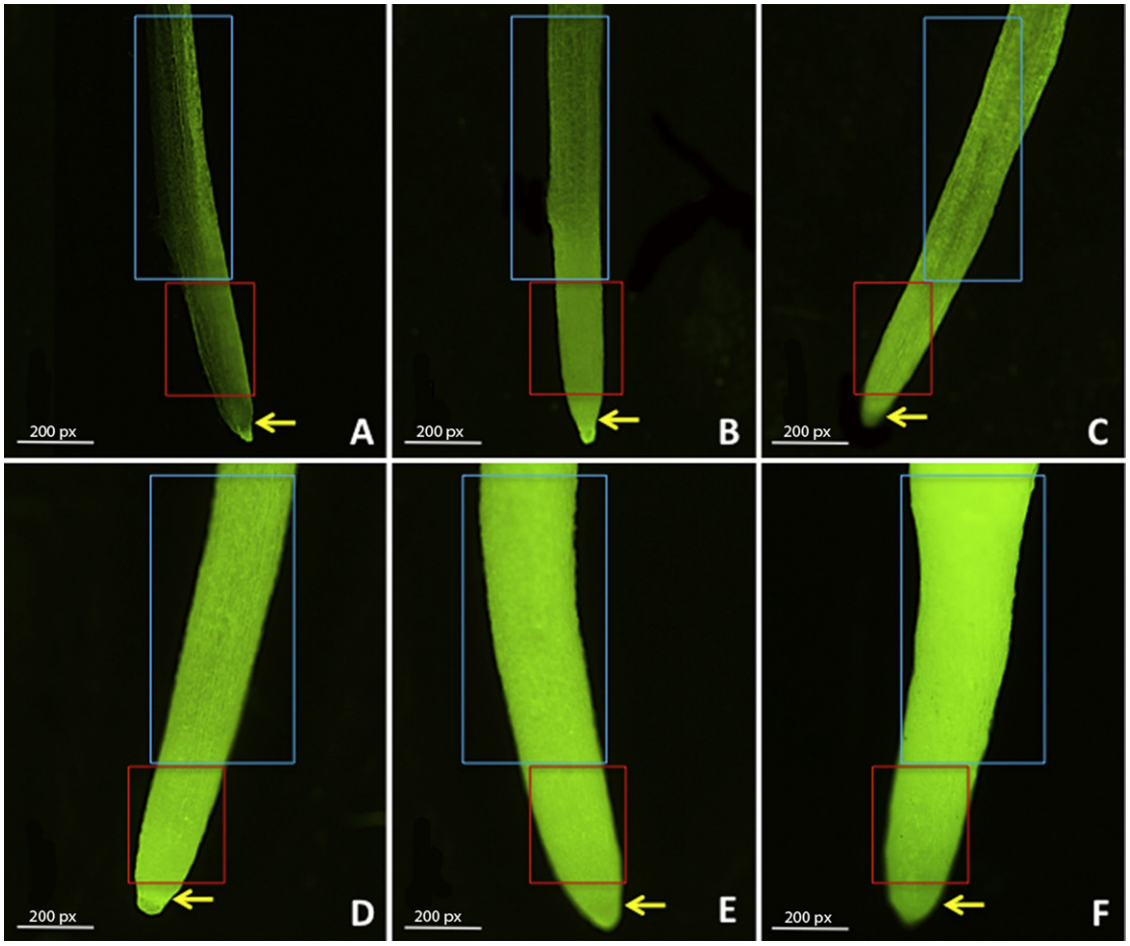

Fig. 4. Depicts ROS generation in seedling roots. Panels A: control, panels (B–F) NiO-NPs 0.25, 0.5, 1.0, 1.5 and 2.0 mg/ml. Root tip, area of elongation and differentiation exhibiting ROS localization are marked with arrow, red and cyan colored boxes, respectively. (For interpretation of the references to color in this figure legend, the reader is referred to the web version of the article.)

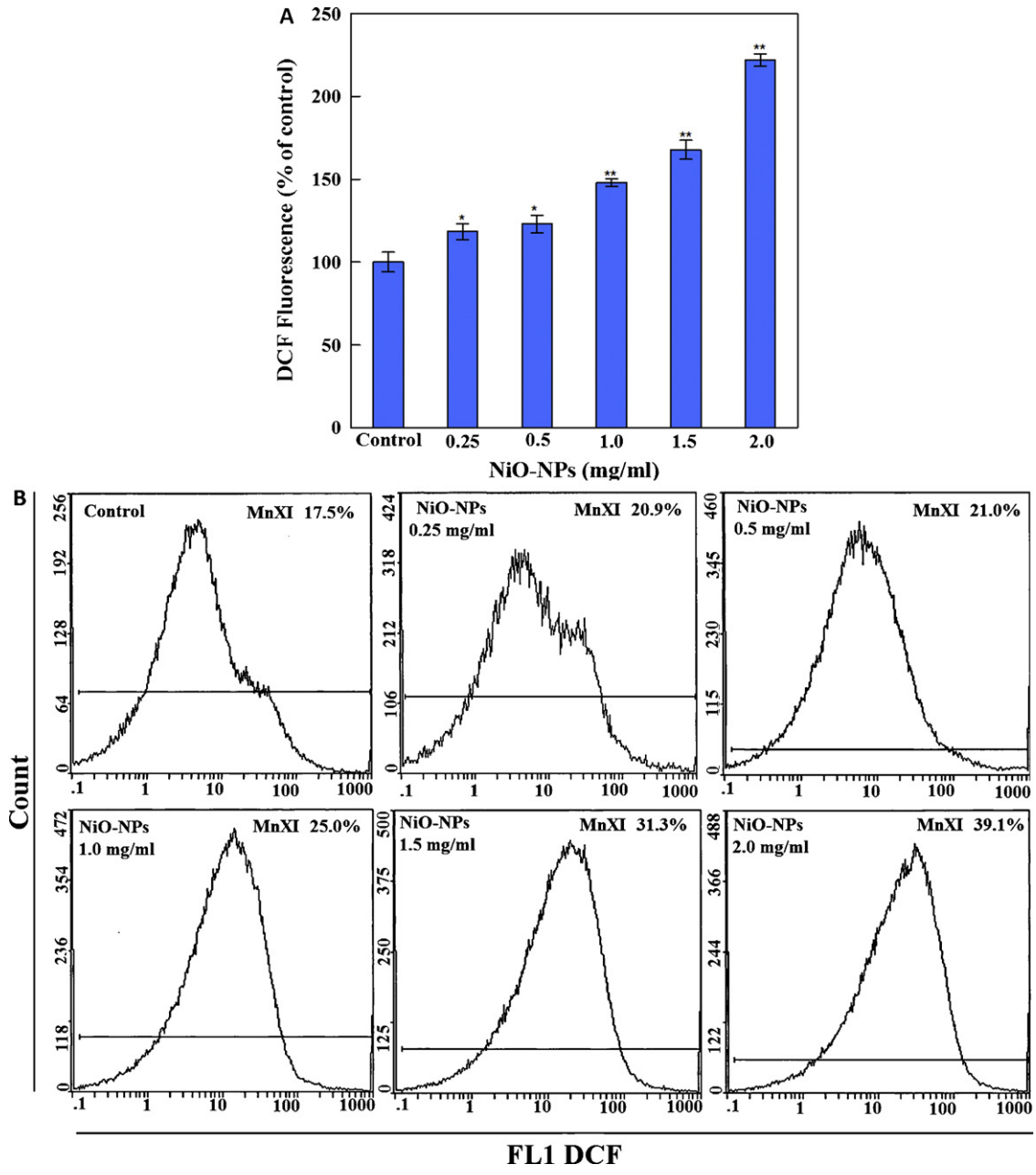

Fig. 5. Flow cytometric analysis of intracellular ROS generation in protoplasts (panel A) ($^{*}p < 0.05$, $^{**}p < 0.01$). Flow images (panel B) showing an enhancement in the DCF fluorescence with increasing NiO-NPs concentrations. MnXI is the fluorescence intensity of DCF.

3.4. Intracellular ROS generation by NiO-NPs

The translocation of NiO-NPs in root cells and dissolution of Ni ions has prompted us to investigate the ROS generation in roots. Staining of roots with DCFH-DA revealed a typical pattern of ROS localization. DCF fluorescence has been used as a marker for oxidative stress and is suggestive of overall oxidative status of a cell [55]. Compared to the untreated control, higher concentrations (1.0, 1.5 and 2.0 mg/ml) of NiO-NPs induced a sharp increase of DCF fluorescence (Fig. 4B–E). Quantitative analysis by flow cytometry revealed higher levels of ROS generation inside the protoplasts. Compared to DCF fluorescence (100%) of control, the treatment doses of 0.25, 0.5, 1.0, 1.5 and 2.0 mg/ml of NiO-NPs resulted in 18%, 23%, 48%, 68% and 122% greater ROS generation (Fig. 5A and B). These results confirmed the oxidative stress in roots as a consequence of NiO-NPs exposure. Earlier studies have also reported oxidative stress in roots of *Brassica oleracea*, and *Oryza sativa* cells, grown under salt stress and MWCNT [28,56]. It has been proposed that the genotoxicity of metals and metal oxides results from non-direct formation of ROS. Abiotic stress (including heavy metals) may result in DNA damage to plant cells either directly or indirectly [57,58]. Indeed, ROS have a potential to react with the cellular components and induce DNA strand breaks, purine oxidations, protein modifications and protein–DNA cross links [59,60]. Thus, higher levels of ROS in NiO-NPs treatment groups might play a critical role in inducing cellular damage leading to apoptotic-like programmed cell death.

3.5. NiO-NPs induced changes in $\Delta\Psi m$

In order to reaffirm the ROS mediated membrane damage, alterations in $\Delta\Psi m$ of tomato roots were analyzed by use of Rh123. Compared to the Rh123 fluorescence in control root, NiO-NPs

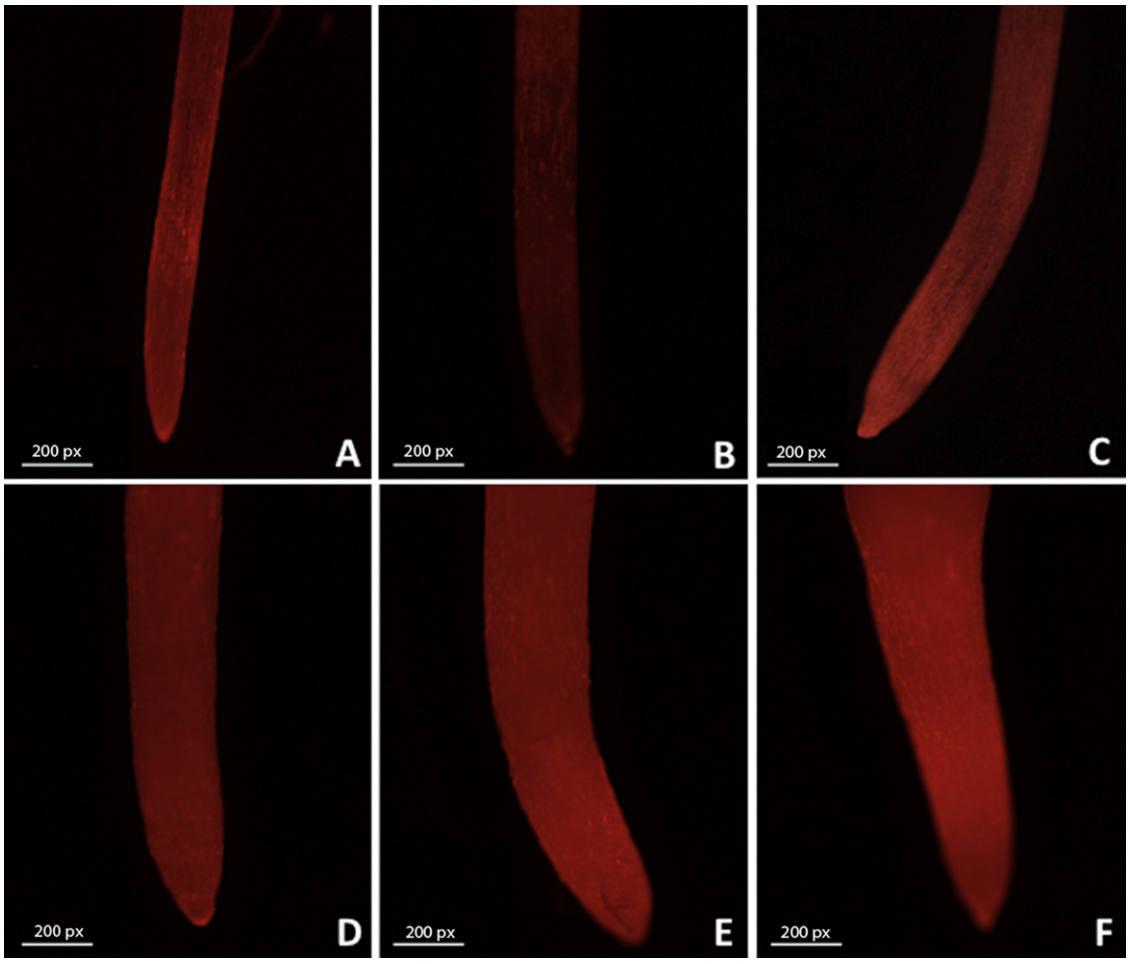

Fig. 6. Rh123 stained roots showing fluorescence decline at 0.25 and 0.5 mg/ml (panels B and C), enhancement at 1.0, 1.5 and 2.0 mg/ml NiO-NPs (panels D–F) and normal bright fluorescence in control (panel A).

(0.25 and 0.5 mg/ml) treatments exhibited discernable reduction of Rh123 fluorescence (Fig. 6A–C). Interestingly, higher concentrations of 1.0, 1.5 and 2.0 mg/ml, a gradual enhancement in fluorescence intensity were observed, possibly due to diffusion into the cytoplasm of cells (Fig. 6D–F). Quantitative evaluation of fluorescence reduction in Rh123 stained protoplasts by flow cytometric analysis revealed 40.1% and 20.4% ($p < 0.01$) reduction in 0.25 and 0.5 mg/ml treated groups as compared with control. However, the protoplasts from1.0, 1.5 and 2.0 mg/ml groups have exhibited an increase in the fluorescence intensity by 5.4%, 28.5% ($p < 0.05$) and 25.4% ($p < 0.01$), respectively (Fig. 7A). The biphasic change in fluorescence intensity with a marked reduction at lower NiO-NPs concentrations followed by fluorescence enhancement through diffusion of Rh123 fluorescence is quite intriguing. The possible reason for fluorescence intensity reduction at lower concentrations of 0.25 and 0.5 mg/ml could be due to dissipation of $\Delta\Psi m$ by disruption of proton-moving force and/or the inner membrane permeability. Thus the relation between greater ROS generation and decline in $\Delta\Psi m$ supports the earlier findings of Liu et al. [40] with water soluble fullerenes. On the contrary, an increase in fluorescence at higher treatment doses relates with the inherent property of mitochondria to swell or shrink in response to changes in $\Delta\Psi m$. Thus the intensity of Rh123 fluorescence changes with the morphological transitions [61]. Altered mitochondria can no longer retain Rh123, which leaks out from the mitochondrial membrane into the cytoplasm mainly by the swelling [62]. Hence, it is concluded that NiO-NPs at lower doses of 0.25 and 0.5 mg/ml dissipate $\Delta\Psi m$, whereas mitochondrial swelling occurs at greater exposure doses of 1.0 to 2.0 mg/ml, leading to leakage of Rh123 to cytosolic components of the treated cells and causing hyperpolarization of the dye. ROS generation within mitochondria occurs in complex I and II of electron transport system through electron leakage, which can directly interact with mitochondrial proteins and lipids, and eventually cause dysfunction [63]. In plants, dissipation of $\Delta\Psi m$ is reported to be an early marker or an essential event in plant apoptosis under various stimuli [64].

The flow cytometric analysis of root protoplast mitochondria revealed two peaks of Rh123 fluorescence, suggestive of a major low fluorescence population (LFP) and a minor high fluorescence population (HFP), accounting for 59% and 31% of the total mitochondria in control. A concentration dependent decline in the percentage of LFP and an increase in HFP been observed. The LFP and HFP at 0.25, 0.5, 1.0, 1.5 and 2.0 mg/ml of NiO-NPs were found to be 59%, 53.8%, 46.8%, 30.6%, 29%, 26% and 31%, 29.4%, 42.3%, 58.4%, 61.5%, 64%, respectively (Fig. 7B). These results correspond with the earlier reports on *Zea mays* leaves and *Oryza sativa* seedlings, where two discrete fluorescence peaks of Rh123 stained mitochondria were recorded due to the presence of two distinct physiological forms of mitochondria [65,66]. It has been suggested that the HFP represents an immature mitochondrial form that may be transformed into the LFP by the incorporation of newly synthesized structural and functional components during mitochondrial membrane biogenesis [67]. In this study the observed changes from LFP to HFP can be attributed to NiO-NPs induced oxidative stress in

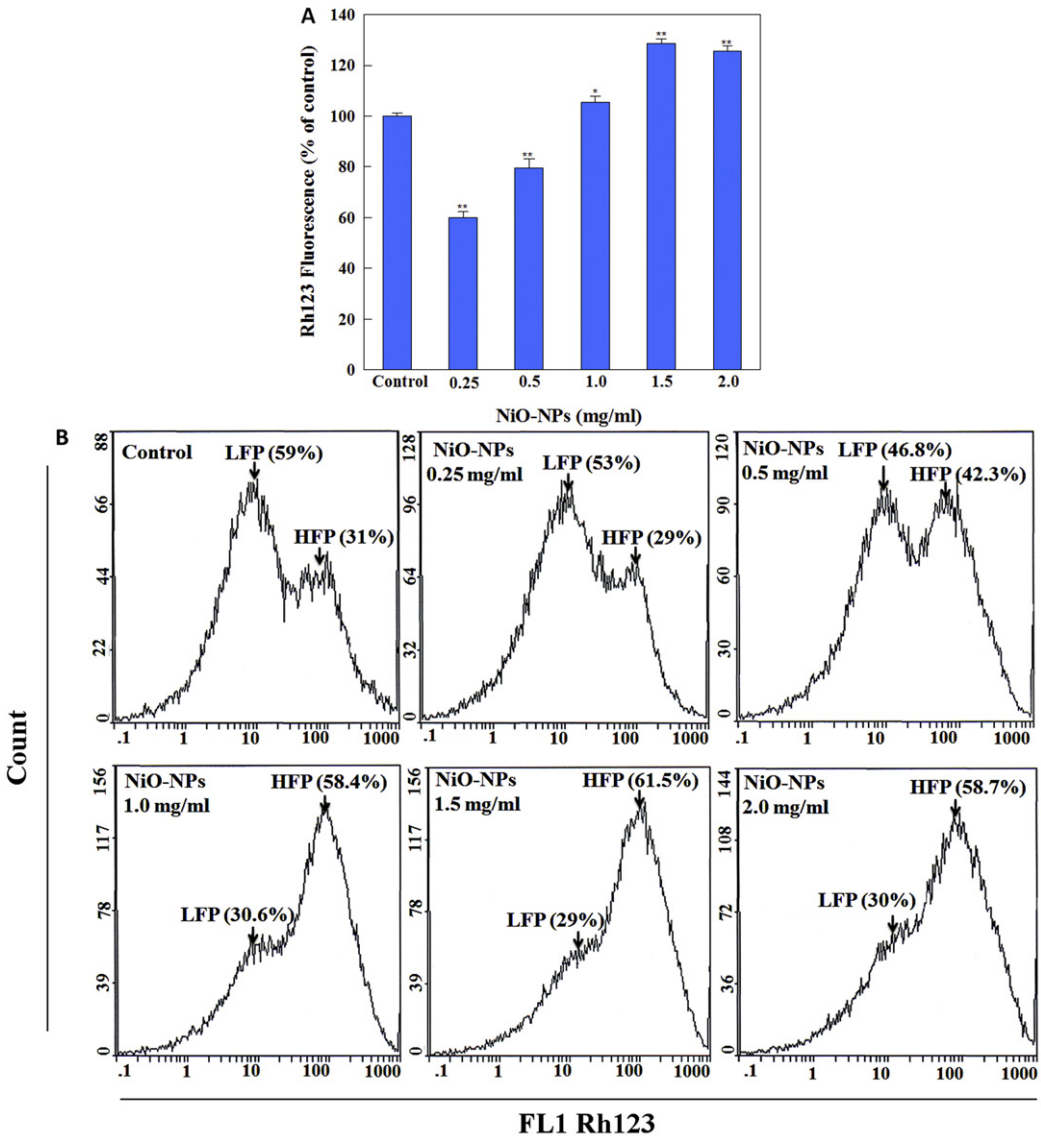

Fig. 7. Flow cytometric assessment of mitochondrial membrane potential in tomato protoplasts. Each histogram in panel A represents mean ± S.D. of Rh123 fluorescence (MnXI) obtained from 50,000 protoplasts in three independent experiments (*$p < 0.05$ vs. control). Panel B shows a major low fluorescence population (LFP) and minor high fluorescence population (HFP) of mitochondria in tomato seedling roots. A concentration dependent decline in LFP with concomitant increase in HFP is indicated by the Rh123 fluorescence (%).

mitochondria of tomato roots, which could be most likely due to disordered F_0F_1-ATPase activity suggested under oxidative stress [66].

3.6. NiO-NPs modulate the antioxidant defense system of tomato roots

In order to assess the extent of oxidative stress in NiO-NPs treated roots, the levels of antioxidant markers such as SOD, CAT and total GSH were determined. The data revealed the basal activity of SOD as 2.4 U/ml in control, whereas, the treatment groups from 0.25 to 2.0 mg/ml of NiO-NPs have exhibited 3.4, 3.8, 5.3, 5.0 and 4.3 U/ml SOD activity. The results suggested a relatively lesser SOD activity at 1.5 and 2.0 mg/ml NiO-NPs (Fig. 8A). Similarly, CAT activity in control was 12.7 (nmol/min/ml), which showed an elevated trend with increasing NiO-NPs concentrations. An enhancement in CAT activity was determined to be 40.7, 70.6 and 91.2 (nmol/min/ml) at 0.5, 1.0 and 1.5 mg/ml, respectively (Fig. 8B). At the highest concentration of 2.0 mg/ml, the CAT activity was reduced to 86.5 (nmol/min/ml). The total GSH levels in seedling roots at 0.25, 0.5 and 1.0 mg/ml treatment groups were determined to be 0.6, 1.6 and 2.8 μM, as compared to 0.06 μM in control (Fig. 8C). However, seedling roots grown at 1.5 and 2.0 mg/ml of NiO-NPs exhibited lesser accumulation (2.4 and 2.3 μM) of total GSH. These results corroborate well with the recent reports on SOD, CAT and GSH activities in the roots of various plants exposed to NPs [68–70]. Plants under the abiotic and biotic stress conditions are reported to increase the production of ROS. For protection against the toxic effects of ROS, plant cells employ antioxidant defense systems, particularly the SOD, CAT and GSH, which provides the first line of defense toward any kind of oxidative toxicity at the cellular level [71]. Increased level of ROS at higher NiO-NPs concentrations of 1.5 and 2.0 mg/ml indicates that the activities of antioxidant enzymes are compromised and oxidative stress occurs due to decreased defense capability [46].

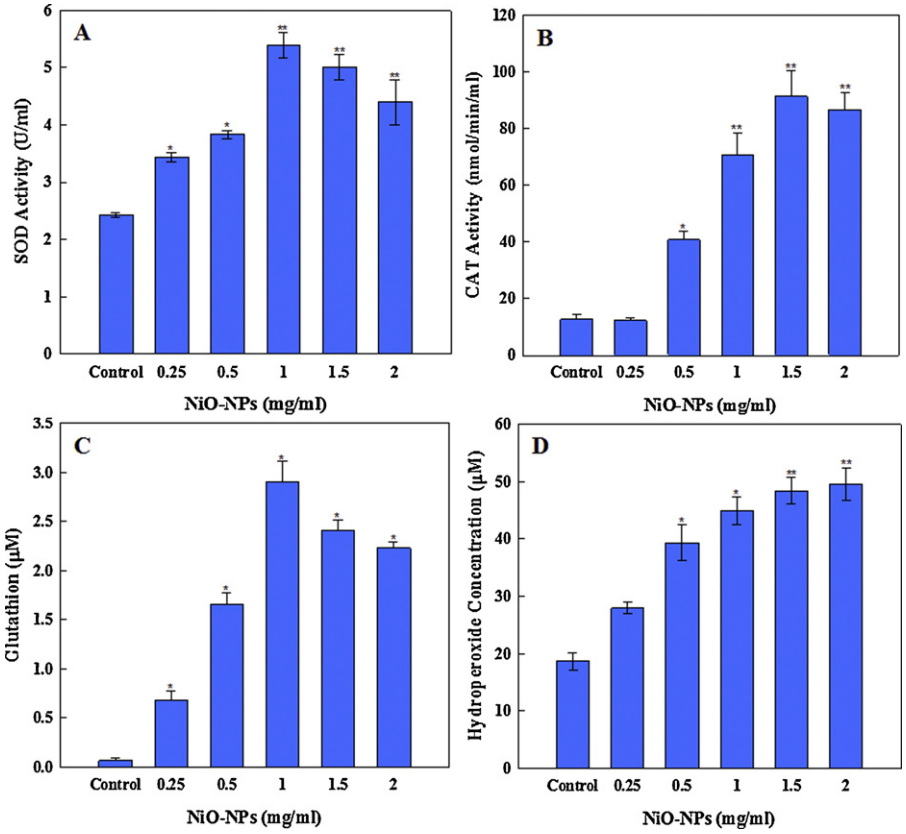

Fig. 8. Effect of NiO-NPs treatments on SOD (panel A), CAT (panel B), GSH (panel C) and LPO (panel D) (*$p < 0.05$, **$p < 0.01$ vs. control).

3.7. NiO-NPs induced LPO in seedling roots

ROS are known to cause lipid peroxidation that promotes degradation of cellular membranes, other lipid structures and yield byproducts that damage DNA [72,73]. Therefore, LPO level in NiO-NPs treated root cells was estimated as an index of oxidative damage to the membranes. Compared to 18.6 μM basal level of LPO in control, NiO-NPs treatment exhibited 39.3, 44.8, 48.4 and 49.5 μM LPO at 0.5, 1.0, 1.5 and 2.0 mg/ml, respectively (Fig. 8D). The concentration dependent increase in the LPO formation in our study strongly supports the recent findings of Wang et al. [69], who have reported that *Lolium perenne* and *Cucurbita pepo* roots grown in the presence of magnetite (Fe_3O_4) NPs exhibited 218% and 259% increase in LPO over control, however, a much greater concentration of 100 mg/l of (Fe_3O_4) NPs was used. Similarly, *Allium cepa* roots grown in the presence of 4 mM TiO_2-NPs have also showed 4.5 times greater level of LPO [74]. The peroxidation of lipids occur both in the cellular and organelle membranes, when the ROS level traverse the threshold limit, and eventually affect the normal cellular functioning, due to increased oxidative stress and release of lipid-derived radicals [71,75] which often results in DNA damage [73].

3.8. NiO-NPs induced apoptosis/necrosis

Comet assay results revealed an atypical pattern of nuclear DNA damage in NiO-NPs treatment groups. Instead of forming a typical comet tail, a hazy (apoptotic) or radially diffused (necrotic) nuclear DNA patterns were invariably observed (Fig. 9C–D). However, the control cells exhibited sharp boundary of nuclear head DNA (Fig. 9A) under identical conditions. The lack of a typical comet tail in cells from different treatment groups, unlike the positive control (EMS 2 mM) has precluded the quantitative analysis of data in terms of Olive tail moment (OTM) and tail length (μm). Therefore, the scoring criteria suggested by Singh [33] were followed for determining the concentration dependent increase in the percentage of apoptotic and necrotic cells in NiO-NPs treated groups. Singh [33] has reported a similar pattern of DNA diffusion and manually categorized the apoptotic or necrotic cells through visual observations. The results indicated 1.3, 2.0, 2.4 and 3.1-fold ($p < 0.01$) increase in the number of apoptotic cells at 0.5, 1.0, 1.5 and 2.0 mg/ml. Also, an increase of 1.8 ($p < 0.05$), 2.0 and 2.5-fold ($p < 0.01$) in necrotic cells were observed at concentrations of 1.0, 1.5 and 2.0 mg/ml (Table 2). Under the identical conditions, the DNA damage in EMS treated (positive control) nuclei exhibited a typical comet tail (Fig. 9B), and the strand breaks were quantitated in terms of OTM (8.5 ± 0.39, arbitrary unit) and tail length (43.2 ± 2.3 μm). An earlier report on NPs induced DNA damage in *Allium cepa* by comet assay also suggested ~3.5-fold greater tail DNA, when exposed to 4 mM TiO_2-NPs [74]. A recent

Table 2
Assessment of NiO-NPs induced apoptosis in tomato root cells by comet assay.

Groups	Percentage apoptotic cells	Percentage necrotic cells
Control	7.00 ± 0.36	0.96 ± 0.20
NiO-NPs (mg/ml)		
0.25	7.33 ± 0.25	1.10 ± 0.26
0.5	9.59 ± 0.66**	1.31 ± 0.21
1.0	14.31 ± 0.75**	1.76 ± 0.30*
1.5	16.86 ± 0.70**	1.94 ± 0.36**
2.0	21.82 ± 0.73**	2.40 ± 0.26**

Each determination was done in three independent experiments and the data represent mean ± S.D. as a percentage of 1000 cells. Statistical analysis was done by one way ANOVA (Dunnett's multiple comparison test).
* $p < 0.05$.
** $p < 0.01$ vs. control.

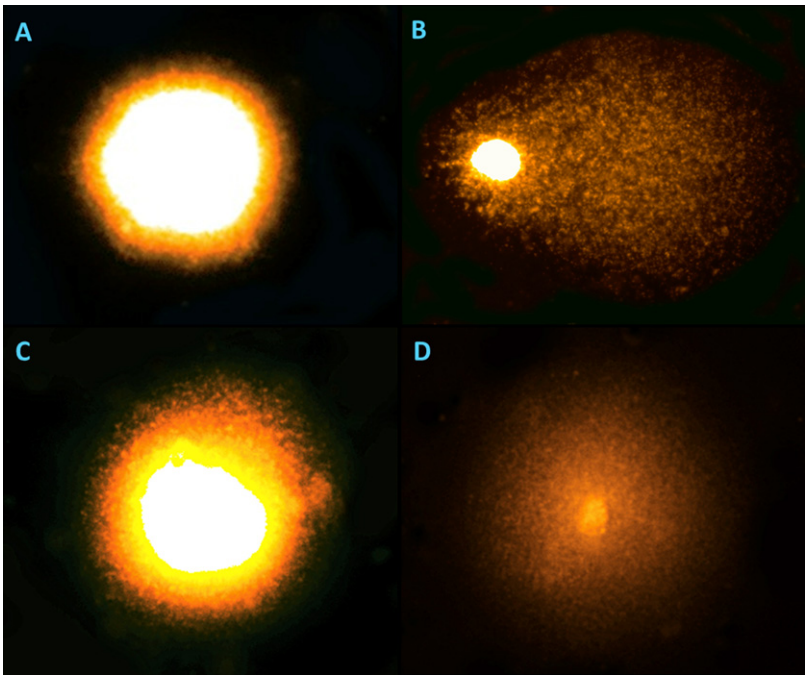

Fig. 9. Comet images of control (panel A), EMS (2 mM) (panel B) and apoptotic and necrotic nuclei from 2.0 mg/ml NiO-NPs treatment group (panel C and D).

report on CuO-NPs induced plant DNA damage has suggested the accumulation of oxidative mutagenic DNA lesions (7,8-dihydro-8-oxoguanine; 2,6-diamino-4-hydroxy-5-formamidopyrimidine; 4,6-diamino-5-formamidopyrimidine) in *Raphanus sativus*, *Lolium perenne*, and *Lolium rigidum* [76]. The development of both apoptotic and necrotic type of cells is the first evidence of cellular and genetic damage elicited in tomato seedling roots, which has indicated that NiO-NPs phytotoxicity leads to plant cell death through the apoptotic and/or necrotic pathways.

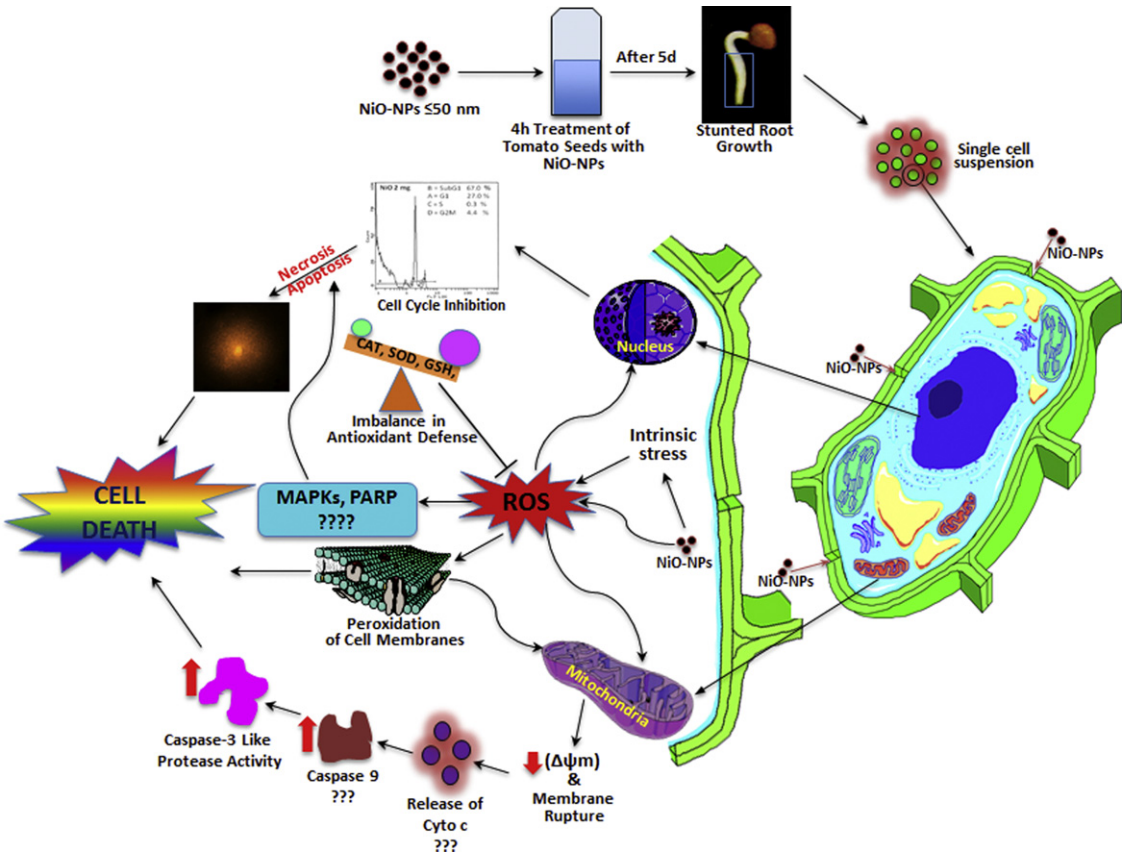

Scheme 1. Plausible mechanism of NiO-NPs induced cellular toxicity in tomato root cell.

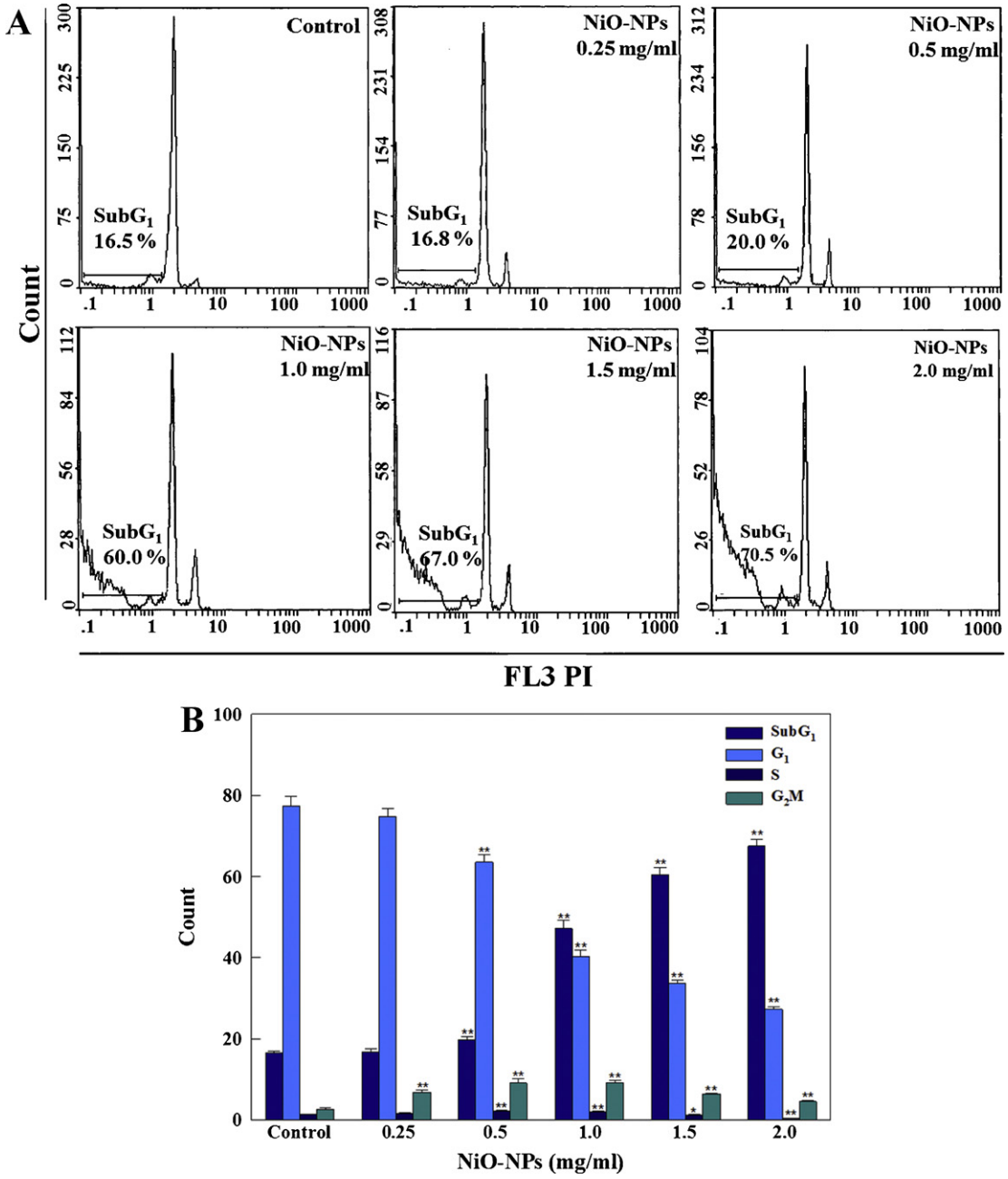

Fig. 10. Cell cycle analysis of PI-stained nuclei of tomato seedling root cells. Panel A shows a representative FACS image exhibiting changes in the progression of normal cell cycle as a function of NiO-NPs concentration. G_1, S, G_2/M represents the percentage of cells present in normal phases of cell cycle, $subG_1$ represents percentage of cells undergone apoptosis/necrosis. Each histogram in panel B represents mean ± S.D. values of different phases of cell cycle obtained from nuclei isolated from 20 roots ($^{*}p < 0.05$, $^{**}p < 0.01$ vs. control).

3.9. Flow cytometric analysis of apoptosis in tomato roots

Cell cycle analysis of PI stained nuclei of control and NiO-NPs treatment groups indicated a concentration dependent increase in the characteristic apoptotic sub-G_1 peak with concomitant reduction in G_1 phase (Fig. 10A). The increase in proportions of apoptotic cells in sub-G_1 phase were determined to be 16.8 ± 0.6, 19.8 ± 0.8, 47.2 ± 2.0, 60.4 ± 1.8 and 67.5 ± 1.7% upon exposure to 0.25, 0.5, 1.0, 1.5 and 2.0 mg/ml of NiO-NPs, respectively. The apoptotic cells in control population were found to be 16.5 ± 0.5%. Similarly, as compared to 2.6 ± 0.3% cells in G_2/M phase of control, greater number of cells (6.8 ± 0.5, 9.1 ± 1.0, 9.1 ± 0.6, 6.4 ± 0.2 and 4.5 ± 0.3%) were found in G_2/M phase of NiO-NPs treated groups, suggesting arrest of cells in this phase (Fig. 10B). Thus, the flow cytometry data confirmed that NiO-NPs are capable of inducing cell death in tomato roots by triggering a cascade of apoptotic events. This is perhaps the first report on G_2/M arrest in root cells of tomato. Our recent study on human amnion epithelial (WISH) cells has also suggested TiO_2-NPs induced G_2/M arrest in cultured human cells [30]. Furthermore, our ongoing studies on cultured human cell lines and rats models with NiO-NPs have also demonstrated the NiO-NPs induced sub-G_1 apoptotic peak, which reaffirmed the possibility of a similar mechanism of PCD in mammalian system and tomato roots. It is widely accepted that apoptotic mechanisms in plants and animals may share common components leading to conserved cellular events [77,78].

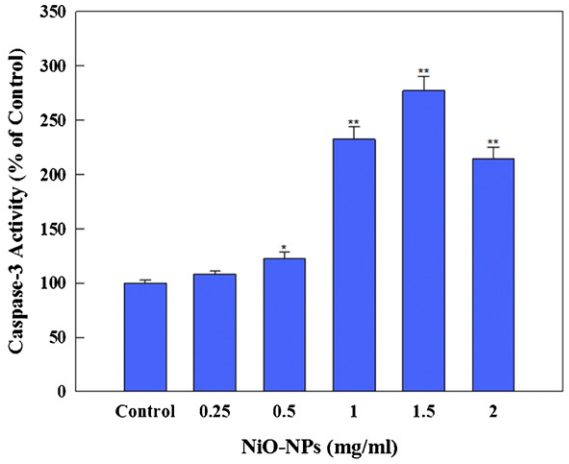

Fig. 11. Effect of NiO-NPs treatment on caspase-3 like protease activity in tomato seedling roots ($^{*}p < 0.05$, $^{**}p < 0.01$ vs. control).

3.10. Effect of NiO-NPs treatments on caspase-3 like protease activity

Activation of caspases plays a critical role in apoptosis and signal transduction. Therefore, caspase-3 activity was assessed in NiO-NPs exposed tomato roots. The data revealed that cytosolic fractions of treated tomato roots showed 1.2, 2.3, 2.7 and 2.1-fold ($p < 0.05$ and $p < 0.01$) greater caspase-3 like protease activity at 0.5, 1.0, 1.5 and 2.0 mg/ml of NiO-NPs, respectively, as compared to the control (Fig. 11). At the highest concentration of 2.0 mg/ml, a decline in caspase-3 activity was observed, which is attributed to cell death via necrosis due to higher toxic effect in roots. So far, no information is available on the NPs induced activation of caspase-3 in tomato plants. Earlier reports, however, suggested the activation of caspase-3 protease by aluminum toxicity and heat shock proteins in *Arabidopsis thaliana* and *Nicotiana tabacum* cells suspensions [79,80]. Plant based studies have suggested that execution of plant apoptosis requires the activation of caspase-like activity [77,78]. Activation of caspase-3 is considered to be the "point-of-no-return" in apoptotic signaling cascade [81]. Thus in this study, significantly higher activity of caspase-3 by the treatment of NiO-NPs elucidated its potential role in triggering apoptotic pathway in plant system.

4. Conclusions

This study provides first evidence on the mechanism of NPs induced toxicity and induction of apoptosis in tomato. Scheme 1 depicts a comprehensive view of the plausible mechanism of cellular toxicity in tomato root cells. It is concluded that a short term exposure of NiO-NPs to tomato seeds resulted in significant repression of root growth and causes oxidative imbalance marked with enhancement in the levels of antioxidant marker enzymes, as a manifestation of phytotoxicity. Ultrastructure analysis revealed the translocation of NiO-NPs in cell cytoplasm with marked changes in organelles structure. The flow cytometry and fluorescence imaging data unequivocally suggests oxidative stress and mitochondrial dysfunction which perhaps stimulated the process of apoptosis. Increased caspase-3 like protease activity reaffirmed the potential of NiO-NPs to trigger intrinsic apoptotic pathway in tomato by releasing Ni ions. Most likely, the root cells exhibiting NPs induced cell death via mitochondrial dependent apoptotic pathway might share common features with those of animal system. Therefore, an in-depth study is warranted to further explore the involvement of other apoptosis related factors, such as caspase-9, cytochrome-c, poly (ADP-ribose) polymerase (PARP), c-Jun N-terminal kinase (JNK) and mitogen-activated protein kinase (MAPK) through transcriptome analysis. Furthermore, it is evident from the present findings that NiO-NPs deserve special attention from the perspective of potential environmental hazards to plants.

Conflict of interest statement

The authors declare that there are no conflicts of interest.

Acknowledgments

Financial support through the National Plan for Sciences and Technology (NPST Project No. 10-NAN1115-02) and Al-Jeraisy Chair for DNA Research Chair, King Saud University, Riyadh, for this study, is greatly acknowledged. The authors also extend their appreciation to the Deanship of Scientific Research at King Saud University for funding the work through the research group project number RGP-VPP-175.

Appendix A. Supplementary data

Supplementary material related to this article found, in the online version, at http://dx.doi.org/10.1016/j.jhazmat.2013.01.063.

References

[1] P. Landa, R. Vankova, J. Andrlova, J. Hodek, P. Marsik, H. Storchova, J.C. White, T. Vanek, Nanoparticle-specific changes in *Arabidopsis thaliana* gene expression after exposure to ZnO, TiO_2, and fullerene soot, J. Hazard. Mater. 241 (2012) 55–62.
[2] B. Nowack, T.D. Bucheli, Occurrence, behavior and effects of nanoparticles in the environment, Environ. Pollut. 150 (2007) 5–22.
[3] E. Navarro, A. Baun, R. Behra, N.B. Hartmann, J. Filser, A.J. Miao, A. Quigg, P.H. Santschi, L. Sigg, Environmental behavior and ecotoxicity of engineered nanoparticles to algae, plants, and fungi, Ecotoxicology 17 (2008) 372–386.
[4] S. Lin, J. Reppert, Q. Hu, J.S. Hudson, M.L. Reid, T.A. Ratnikova, A.M. Rao, H. Luo, P.C. Ke, Uptake, translocation, and transmission of carbon nanomaterials in rice plants, Small 5 (2009) 1128–1132.
[5] D. Lin, B. Xing, Root uptake and phytotoxicity of ZnO nanoparticles, Environ. Sci. Technol. 42 (2008) 5580–5585.
[6] W.M. Lee, Y.J. An, H. Yoon, H.S. Kweon, Toxicity and bioavailability of copper nanoparticles to the terrestrial plants Mung bean (*Phaseolus radiatus*) and Wheat (*Triticum aestivum*): plant agar test for water-insoluble nanoparticles, Environ. Toxicol. Chem. 27 (2008) 1915–1921.
[7] E. Wild, K.C. Jones, Novel method for the direct visualization of *in vivo* nanomaterials and chemical interactions in plants, Environ. Sci. Technol. 43 (2009) 5290–5294.
[8] M.D. Whiteside, K.K. Treseder, P.R. Atsatt, The brighter side of: quantum dots track organic nitrogen through fungi and plants, Ecology 90 (2009) 100–108.
[9] D. Lin, B. Xing, Phytotoxicity of nanoparticles: inhibition of seed germination and root growth, Environ. Pollut. 150 (2007) 243–250.
[10] J.E. Cañas, M. Long, S. Nations, R. Vadan, L. Dai, M. Luo, R. Ambikapathi, E.H. Lee, D. Olszyk, Effects of functionalized and nonfunctionalized single-walled carbon nanotubes on root elongation of select crop species, Environ. Toxicol. Chem. 27 (2008) 1922–1931.
[11] X. Ma, J. Geiser-Lee, Y. Deng, A. Kolmakov, Interactions between engineered nanoparticles (Enps) and plants: phytotoxicity, uptake and accumulation, Sci. Total Environ. 408 (2010) 3053–3061.
[12] K.J. Dietz, S. Herth, Plant nanotoxicology, Trends Plant Sci. 16 (2011) 582–589.
[13] A. Schützendübel, A. Polle, Plant responses to abiotic stresses: heavy metal-induced oxidative stress and protection by Mycorrhization, J. Exp. Bot. 53 (2002) 1351–1365.
[14] S.S. Sharma, K.J. Dietz, The relationship between metal toxicity and cellular redox imbalance, Trends Plant Sci. 14 (2009) 43–50.
[15] H.L. Karlsson, The comet assay in nanotoxicology research, Anal. Bioanal. Chem. 398 (2010) 651–666.
[16] M. Mehrabi, R. Wilson, Intercalating gold nanoparticles as universal labels for DNA detection, Small 3 (2007) 1491–1495.
[17] S. Dey, K. Ghose, D. Basu, Fusarium elicitor-dependent calcium influx and associated ROS generation in tomato is independent of cell death *Fusarium* elicitor-dependent calcium influx and associated ROS generation in tomato is independent of cell death, Eur. J. Plant Pathol. 126 (2010) 217–228.
[18] F. Takahashi, T. Mizoguchi, R. Yoshida, K. Ichimura, K. Shinozaki, Calmodulin-dependent activation of MAP Kinase for ROS homeostasis in *Arabidopsis*, Mol. Cell 41 (2011) 649–660.
[19] T.S. Gechev, J. Hille, Hydrogen peroxide as a signal controlling plant programmed cell death, J. Cell Biol. 168 (2005) 17–20.

[20] T. Karuppanapandian, J.C. Moon, C. Kim, K. Manoharan, W. Kim, Reactive oxygen species in plants: their generation, signal transduction, and scavenging mechanisms, Aust. J. Crop Sci. 5 (2011) 709–725.
[21] K.E. Hammond-Kosack, J.D. Jones, Resistance gene-dependent plant defense responses, Plant Cell 8 (1996) 1773–1791.
[22] V. Houot, P. Etienne, A.S. Petitot, S. Barbier, J.P. Blein, L. Suty, Hydrogen peroxide induces programmed cell death features in cultured tobacco BY-2 cells in a dose-dependent manner, J. Exp. Bot. 52 (2001) 1721–1730.
[23] B.S. Tiwari, B. Belenghi, A. Levine, Oxidative stress increased respiration and generation of reactive oxygen species, resulting in ATP depletion, opening of mitochondrial permeability transition, and programmed cell death, Plant Physiol. 128 (2002) 1271–1281.
[24] N. Gou, A. Onnis-Hayden, A.Z. Gu, Mechanistic toxicity assessment of nanomaterials by whole-cell-array stress genes expression analysis, Environ. Sci. Technol. 44 (2010) 5964–5970.
[25] C. Collazo, O. Chacón, O. Borrás, Programmed cell death in plants resembles apoptosis of animals, Biotechnol. Appl. 23 (2006) 1–10.
[26] E. Corredor, P.S. Testillano, M.J. Coronado, P. González-Melendi, R. Fernández-Pacheco, C. Marquina, M.R. Ibarra, J.M. de la Fuente, D. Rubiales, A. Pérez-de-Luque, M.C. Risueño, Nanoparticle penetration and transport in living pumpkin plants: in situ subcellular identification, BMC Plant Biol. 9 (2009) 45.
[27] C.W. Lee, S. Mahendra, K. Zodrow, D. Li, Y.C. Tsai, J. Braam, P.J.J. Alvarez, Developmental phytotoxicity of metal oxide nanoparticles to *Arabidopsis thaliana*, Environ. Toxicol. Chem. 29 (2010) 669–675.
[28] M. Hernandez, N. Fernandez-Garcia, P. Diaz-Vivancos, E. Olmos, A different role for hydrogen peroxide and the antioxidative system under short and long salt stress in *Brassica oleracea* roots, J. Exp. Bot. 61 (2010) 521–535.
[29] S. Imanishi, J. Momose, I. Hiura, Isolation and culture of *Lycopersicon esculentum* root protoplasts, Plant Tiss. Cul. Lett. 2 (1985) 25–26.
[30] Q. Saquib, A.A. Al-Khedhairy, M.A. Siddiqui, F.M. Abou-Tarboush, A. Azam, J. Musarrat, Titanium dioxide nanoparticles induced cytotoxicity, oxidative stress and DNA damage in human amnion epithelial (WISH) cells, Toxicol. In Vitro 26 (2012) 351–361.
[31] Q. Saquib, J. Musarrat, M.A. Siddiqui, S. Dutta, S. Dasgupta, J.P. Giesy, A.A. Al-Khedhairy, Cytotoxic and necrotic responses in human amniotic epithelial (WISH) cells exposed to organophosphate insecticide phorate, Mutat. Res. 744 (2012) 125–134.
[32] Q. Saquib, A.A. Al-Khedhairy, S. Al-Arifi, A. Dhawan, J. Musarrat, Assessment of methyl thiophanate-Cu (II) induced DNA damage in human lymphocytes, Toxicol. In Vitro 23 (2009) 848–854.
[33] N.P. Singh, A simple method for accurate estimation of apoptotic cells, Exp. Cell Res. 256 (2000) 328–337.
[34] Q. Saquib, S.M. Attia, M.A. Siddiqui, M.A.M. Aboul-Soud, A.A. Al-Khedhairy, J.P. Giesy, J. Musarrat, Phorate-induced oxidative stress, DNA damage and transcriptional activation of P53 and caspase genes in male Wistar rats, Toxicol. Appl. Pharmacol. 259 (2012) 54–65.
[35] B.J. Berne, R. Pecora, Dynamic Light Scattering: With Applications to Chemistry, Biology and Physics, Dover Publications, Mineola, NY, 2000.
[36] V. Sharma, D. Anderson, A. Dhawan, Zinc oxide nanoparticles induce oxidative DNA damage and ROS-triggered mitochondria mediated apoptosis in human liver cells (HepG2), Apoptosis 17 (2012) 852–870.
[37] N. Singh, G.J.S. Jenkins, B.C. Nelson, B.J. Marquis, T.G.G. Maffeis, A.P. Brownd, P.M. Williams, C.J. Wright, S.H. Doak, The role of iron redox state in the genotoxicity of ultrafine superparamagnetic iron oxide nanoparticles, Biomaterial 33 (2012) 163–170.
[38] P. Boonyanitipong, B. Kositsup, P. Kumar, S. Baruah, J. Dutta, Toxicity of ZnO and TiO_2 nanoparticles on germinating rice seed *Oryza sativa* L, Int. J. Biosci. Biochem. Bioinform. 1 (2011) 282–285.
[39] D. Stampoulis, S.K. Sinha, J.C. White, Assay-dependent phytotoxicity of nanoparticles to plants, Environ. Sci. Technol. 43 (2009) 9473–9479.
[40] Q. Liu, Y. Zhao, Y. Wan, J. Zheng, X. Zhang, C. Wang, X. Fang, J. Lin, Study of the inhibitory effect of water-soluble fullerenes on plant growth at the cellular level, ACS Nano 4 (2010) 5743–5748.
[41] M.V. Khodakovskaya, E. Dervishi, M. Mahmood, Y. Xu, Z. Li, F. Watanabe, A.S. Biris, Carbon nanotubes are able to penetrate plant seed coat and dramatically affect seed germination and plant growth, ACS Nano 3 (2009) 3221–3227.
[42] M.V. Khodakovskaya, K. de Silva, A.S. Biris, E. Dervishi, H. Villagarcia, Carbon nanotubes induce growth enhancement of tobacco cells, ACS Nano 6 (2012) 2128–2135.
[43] L. Zheng, F. Hong, S. Lu, C. Liu, Effect of nano-TiO_2 on strength of naturally and growth aged seeds of spinach, Biol. Trace Elem. Res. 104 (2005) 83–91.
[44] United States Environment Protection Agency. 1996. Ecological effects test guidelines (OPPTS 850.4200) Seed Germination Root Elongation Toxicity Test. Available from: http://www.docstoc.com/docs/46344082/8504200—Seed-GerminationRoot-Elongation-Toxicity-Test-(PDF) (last assessed on 22.09.12).
[45] S.G. Wu, L. Huang, J. Head, D.R. Chen, I.C. Kong, Y.J. Tang, Phytotoxicity of metal oxide nanoparticles is related to both dissolved metals ions and adsorption of particles on seed surfaces, J. Pet. Environ. Biotechnol. 3 (2012) 126, http://dx.doi.org/10.4172/2157-7463.1000126.
[46] S. Lee, S. Kim, S. Kim, I. Lee, Assessment of phytotoxicity of ZnO NPs on a medicinal plant, *Fagopyrum esculentum*, Environ. Sci. Pollut. Res. (2012), http://dx.doi.org/10.1007/s11356-012-1069-8.
[47] M. de Felipe, M.M. Lucas, J.M. Pozuelo, Cytochemical study of catalase and peroxidase in the mesophyll of *Lolium rigidum* plants treated with isoproturon, J. Plant Physiol. 132 (1988) 67–73.
[48] M. Ferreira, B. Bird, D.D. Davies, The effect of light on the structure and organization of Leman peroxisomes, J. Exp. Bot. 40 (1989) 1029–1035.
[49] J.M. Palma, M. Garrido, M.I. Rodriguez-Garcia, L.A. del Rio, Peroxisome proliferation and oxidative stress mediated by activated oxygen species in plant peroxisomes, Arch. Biochem. Biophys. 287 (1991) 68–74.
[50] E. Oksanen, E. Haikio, J. Sober, D.F. Karnosky, Ozone-induced H_2O_2 accumulation in field-grown aspen and birch is linked to foliar ultrastructure and peroxisomal activity, New Phytol. 161 (2003) 791–799.
[51] A. Chelstowska, R.A. Butow, RTG genes in yeast that function in communication between mitochondria and the nucleus are also required for expression of genes encoding peroxisomal proteins, J. Biol. Chem. 270 (1995) 18141–18146.
[52] C.B. Epstein, J.A. Waddle, W.I.V. Hale, V. Davé, J. Thornton, T.L. Macatee, H.R. Garner, R.A. Butow, Genome-wide responses to mitochondrial dysfunction, Mol. Biol. Cell 12 (2001) 297–308.
[53] J. Torreilles, M.C. Guerin, Nickel(II) as a temporary catalyst for hydroxyl radical generation, FEBS Lett. 272 (1990) 58–60.
[54] C.B. Klein, K. Frenkel, M. Costa, The role of oxidative processes in metal carcinogenesis, Chem. Res. Toxicol. 4 (1991) 592–604.
[55] H. Wang, J.A. Joseph, Quantifying cellular oxidative stress by dichlorofluorescein assay using microplate reader, Free Radic. Biol. Med. 27 (1999) 612–616.
[56] X. Tan, C. Lin, B. Fugetsu, Studies on toxicity of multi-walled carbon nanotubes on suspension rice cells, Carbon 47 (2009) 3479–3487.
[57] H. Zhang, Y. Jiang, Z. He, M. Ma, Cadmium accumulation and oxidative burst in garlic (*Allium sativum*), J. Plant Physiol. 162 (2005) 977–984.
[58] M. Kumari, A. Mukherjee, N. Chandrasekaran, Genotoxicity of silver nanoparticles in *Allium cepa*, Sci. Total Environ. 407 (2009) 5243–5246.
[59] K.B. Beckman, B.N. Ames, Oxidative decay of DNA, J. Biol. Chem. 272 (1997) 19633–19636.
[60] B.S. Berlett, E.R. Stadtman, Protein oxidation in aging, disease, and oxidative stress, J. Biol. Chem. 272 (1997) 20313–20316.
[61] P.X. Petit, Flow cytometric analysis of rhodamine 123 fluorescence during modulation of the membrane potential in plant mitochondria, Plant Physiol. 98 (1992) 279–286.
[62] G. Ouédraogo, P. Morlière, R. Santus, M.A. Miranda, J.V. Castell, Damage to mitochondria of cultured human skin fibroblasts photosensitized by fluoroquinolones, Photochem. Photobiol. B 58 (2000) 20–25.
[63] H.P. Indo, M. Davidson, H.C. Yen, S. Suenaga, K. Tomita, T. Nishii, M. Higuchi, Y. Koga, T. Ozawa, H.J. Majima, Evidence of ROS generation by mitochondria in cells with impaired electron transport chain and mitochondrial DNA damage, Mitochondrion 7 (2007) 106–118.
[64] N. Yao, B.J. Eisfelder, J. Marvin, J.T. Greenberg, The mitochondrion-an organelle commonly involved in programmed cell death in *Arabidopsis thaliana*, Plant J. 40 (2004) 596–610.
[65] J. Yang, L. Ma, Y. Zhang, F. Fang, L. Li, Flow cytometric identification of two different rhodamine-123-stained mitochondrial populations in maize leaves, Protoplasma 231 (2007) 249–252.
[66] C. Hu, Q. Sun, X. Peng, Q. Huang, M. Wang, S. Li, Y. Zhu, Flow cytometric analysis of mitochondrial populations in HL-CMS systems of rice under H_2O_2 Stress, Protoplasma 241 (2010) 91–98.
[67] C. Lopez-Mediavilla, A. Orfao, J. San Miguel, J.M. Medina, Developmental changes in rat liver mitochondrial populations analyzed by flow cytometry, Exp. Cell Res. 203 (1992) 134–140.
[68] S. Kim, S. Lee, I. Lee, Alteration of phytotoxicity and oxidant stress potential by metal oxide nanoparticles in *Cucumis Sativus*, Water Air Soil Pollut. 223 (2012) 2799–2806.
[69] H. Wang, X. Kou, Z. Pei, J.Q. Xiao, X. Shan, B. Xing, Physiological effects of magnetite (Fe_3O_4) nanoparticles on perennial ryegrass (*Lolium perenne* L.) and pumpkin (*Cucurbita mixta*) plants, Nanotoxicology 5 (2011) 30–42.
[70] N.E. Estrella-Gómeza, E. Sauri-Duchb, O. Zapata-Pérezc, J.M. Santamaría, Glutathione plays a role in protecting leaves of *Salvinia minima* from Pb^{2+} damage associated with changes in the expression of Smgs genes and increased activity of GS, Environ. Exp. Bot. 75 (2012) 188–194.
[71] S.S. Gill, N. Tuteja, Reactive oxygen species and antioxidant machinery in abiotic stress tolerance in crop plants, Plant Physiol. Biochem. 48 (2010) 909–930.
[72] A.W. Girotti, Lipid hydroperoxide generation, turnover, and effector action in biological systems, J. Lipid Res. 39 (1998) 1529–1542.
[73] N. Tuteja, M.B. Singh, M.K. Misra, P.L. Bhalla, R. Tuteja, Molecular mechanisms of DNA damage and repair: progress in plants, Crit. Rev. Biochem. Mol. Biol. 36 (2001) 337–397.
[74] M. Ghosh, M. Bandyopadhyay, A. Mukherjee, Genotoxicity of titanium dioxide (TiO_2) nanoparticles at two trophic levels: plant and human lymphocytes, Chemosphere 81 (2010) 1253–1262.
[75] J.L. Montillet, S. Chamnongpol, C. Rustérucci, J. Dat, B. van de Cotte, J.P. Agnel, C. Battesti, D. Inzé, F.V. Breusegem, C. Triantaphylides, Fatty acid hydroperoxides and H_2O_2 in the execution of hypersensitive cell death in tobacco leaves, Plant Physiol. 138 (2005) 1516–1526.
[76] D.H. Atha, H. Wang, E.J. Petersen, D. Cleveland, R.D. Holbrook, P. Jaruga, M. Dizdaroglu, B. Xing, B.C. Nelson, Copper oxide nanoparticle mediated DNA damage in terrestrial plant models, Environ Sci Technol. 46 (2012) 1819–1827.
[77] O. del Pozo, E. Lam, Caspases and programmed cell death in the hypersensitive response of plants to pathogens, Curr. Biol. 88 (1998) 1129–1132.

[78] P. Mlejnek, S. Prochazka, Activation of caspase-like proteases and induction of apoptosis by isopentenyladenosine in tobacco BY-2 cells, Planta 215 (2002) 158–166.
[79] Z. Li, D. Xing, Mechanistic study of mitochondria-dependent programmed cell death induced by aluminium phytotoxicity using fluorescence techniques, J. Exp. Bot. 62 (2011) 331–343.
[80] R.H. Tian, G.Y. Zhang, C.H. Yan, Y.R. Dai, Involvement of poly(ADP-ribose) polymerase and activation of caspase-3-like protease in heat shock-induced apoptosis in tobacco suspension cells, FEBS Lett. 474 (2000) 11–15.
[81] D.R. Green, G.P. Amarante-Mendes, The point-of-no-return: mitochondria, caspases and the commitment to cell death, Cell Differ. 24 (1998) 45–61.